Phospholipid interactions in model membrane systems
II. Theory

Dirk Stigter,* James Mingins‡, and Ken A. Dill*
*Department of Pharmaceutical Chemistry, University of California, San Francisco, California 94143 USA; ‡Agriculture and Food Research Council Institute of Food Research, Norwich Laboratory, Colney Lane, Norwich, NR4 7UA, United Kingdom

ABSTRACT We describe statistical thermodynamic theory for the lateral interactions among phospholipid head groups in monolayers and bilayers. Extensive monolayer experiments show that at low surface densities, PC head groups have strong lateral repulsions which increase considerably with temperature, whereas PE interactions are much weaker and have no significant temperature dependence (see the preceding paper). In previous work, we showed that the second virial coefficients for these interactions can be explained by: (*a*) steric repulsions among the head groups, and (*b*) a tilting of the P^-N^+ dipole of PC so that the N^+ end enters the oil phase, to an extent that increases with temperature. It was also predicted that PE interactions should be weaker and less temperature dependent because the N^+ terminal of the PE head-group is hydrophilic, hence, it is tilted into the water phase, so dipolar contributions among PE's are negligible due to the high dielectric constant of water. In the present work, we broaden the theory to treat phospholipid interactions up to higher lateral surface densities. We generalize the Hill interfacial virial expansion to account for dipoles and to include the third virial term. We show that to account for the large third virial coefficients for both PC and PE requires that the short range lateral attractions among the head groups also be taken into account. In addition, the third virial coefficient includes fluctuating head group dipoles, computed by Monte Carlo integration assuming pairwise additivity of the instantaneous pair potentials. We find that because the dipole fluctuations are correlated, the average triplet interactions do not equal the sum of the average dipole pair potentials. This is important for predicting the magnitude and the independence of temperature of the third virial coefficients for PC. The consistency of the theory with data of both the second and the third virial coefficients extends the applicability of the head-group model to semiconcentrated monolayers, in agreement with the surface potential data in the foregoing paper.

INTRODUCTION

The stabilities, structures, and phase changes in phospholipid monolayers and bilayer membranes arise from the lateral interactions among the phospholipid molecules. These forces probably also play a role in association and fusion of membranes, and in the incorporation and transport of molecules across membranes. The lateral interactions among phospholipids are the sum of interactions from both the head groups and the alkyl chains. Because the behavior of phosphatidylcholine (PC) and phosphatidylethanolamine (PE) molecules are so different, a large component of these lateral interactions must come from the head groups. The experimental method of choice for studying the interactions among phospholipid head groups is that of pressure-area isotherms at the oil/water interface, for reasons described in the preceding companion paper (1): the surface density can be controlled over a wide range, and at low to intermediate coverages the alkyl chain interactions are small so the head groups can be studied in isolation. Previous discussions of experiments (2, 3) have focussed on head-group interactions at low surface densities. However, to ultimately understand the behavior of bilayers, vesicles, and biomembranes, it is necessary for theory and experiment to address the problem of lateral interactions at higher surface densities. The present work is intended as a step in this direction. In the preceding companion paper, reliable experimental pressure-area isotherms are presented for different phospholipids at the oil/water interface covering a broad range of surface densities from low to intermediate. From those data we have determined the second and third virial coefficients and their temperature dependences. In the present paper, we describe a simple statistical mechanical theory that predicts the lateral interactions of phospholipid head groups over the same range from low to intermediate surface densities. It predicts well the second and third virial coefficients and their temperature dependences for PC and PE head groups.

The most rigorous theoretical approach to intermolecular interactions for low to intermediate densities either in three dimensional or two dimensional systems is through the method of the virial expansion. Previously, a simple statistical mechanical theory has been developed (3). From that effort it was concluded that the second virial coefficient and its temperature dependence could be predicted by a simple model in which the head group is considered to be a rigid P^-N^+ dipole, with the P^- fixed at the interface and the N^+ end free to tilt relative to the

0006-3495/92/06/1616/14 $2.00

plane of the interface. Electrostatics drive the N^+ toward the water phase, but the hydrophobic interaction drives the cluster of methyl groups at the N^+ end of PC toward the oil phase. Orientational fluctuations are predicted to be large, with the equilibrium orientation of the N^+ end of PC slightly into the oil phase, increasing with temperature. Because of the low dielectric constant of the oil phase, this leads to strong lateral repulsion among PC molecules increasing with temperature. Because PE does not have a hydrophobic cluster of methyls at the N^+ end of the dipole, it is predicted to orient toward the water phase, with much less lateral repulsion and negligible temperature dependence (3).

The purpose of the present paper is to develop more general theory to treat the broader range of surface densities, from low to intermediate to account for both the second and third virial coefficients, B_2 and B_3; the previous effort treated only low surface densities and the second virial coefficients. Toward this end, we first require the virial expansion for interfacial pressure-area processes. We obtain this by generalization of a treatment of T. L. Hill (4); see Appendix A. The extension of the earlier work (2, 3), undertaken to confirm and fortify the models of PE and PC summarized above, has several new features. The new, more accurate experimental values of B_3 and their temperature dependence (1) put very serious restraints on any head group model and we now have to consider more interactions than before. Apart from steric repulsion and dipole interactions we now have to introduce hydrogen bonding between PE and hydrophobic interaction between PC head groups in water. The microscopic modeling of these attractive interactions is necessarily approximate. In the earlier model of B_2 the large dielectric asymmetry of the oil/water interface and out-of-plane head-group fluctuations were necessary ingredients of the dipole interaction. This is confirmed in the present analysis. Correlations among such head-group fluctuations are new and essential aspects in fitting the B_3 data.

VIRIAL COEFFICIENTS FOR STERIC AND DIPOLAR INTERACTIONS

The virial expansion describing the lateral pressure, Π, required to hold a monolayer in equilibrium, is given in terms of the surface concentration Γ by

$$\frac{\Pi}{kT} = \Gamma + B_2\Gamma^2 + B_3\Gamma^3 \ldots, \qquad (1)$$

where B_2 and B_3 are the second and third virial coefficients respectively, and kT is Boltzmann's constant multiplied by the absolute temperature. Experiments permit the determination of the virial coefficients B_2 and B_3, as described in the preceding paper (1).

The virial coefficients provide insight into the molecular interactions since they are directly related to the intermolecular potentials. Joslin (5) has treated this relation for the virial coefficients B_2 and B_3 of a surface film of hard disc dipoles without, however, allowing for dipole fluctuations or additional interactions. We find that phospholipid monolayers require a more general model than considered by Joslin; the formal development is given in Appendix A. Experiments in the preceding paper show that at low to intermediate surface densities, only the head group interactions among phospholipids contribute to the second and third virial coefficients; the chain interactions contribute only at higher densities. Two types of head group interaction contribute to the virial coefficients. The first is the adsorption potential, u_i and u_j of the head groups of molecules i and j; these are the forces restraining molecular motion normal to the interface. The other important contribution to the virial coefficients is that of the lateral interactions, u_{ij} between pairs of molecules and u_{ijk} among triplets. The relationships between these interaction potentials and the virial coefficients B_2 and B_3 is given in Appendix A. Our purpose here is to explore various possible models for the intermolecular interactions, to then predict second and third virial coefficients, and to compare theory and experiment to reject or establish what models are consistent with the data.

We first consider the dipolar contributions to the lateral head-group interactions. We assume the dipole interactions are pairwise additive. Then for the triplet interaction in Fig. 1 and Eq. A24,

$$u_{123}(R, s, r) = u_{12}(R) + u_{13}(s) + u_{23}(r). \qquad (2)$$

As in the earlier model of the P^-N^+ head-group dipole (3) with a PN distance of 4.5 Å, we make the reasonable assumption that the P^- charge is held at the heptane/water interface and that the N^+ charge may be either in the heptane or in the water. Because it has previously been found (2) that the in-plane dipole components lead to only a very small average attraction (see below), we

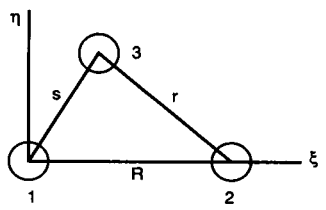

FIGURE 1 Coordinates for triplet of head groups at $\eta\xi$ interface.

have neglected the in-plane dipole contributions in most of our present computations. We focus on the out-of-plane dipole components; these are shown schematically in Fig. 2. If both dipolar charges are in the oil phase (see Fig. 2 *a*), the pair potential u_{12} between two dipoles in oil is well approximated by (2),

$$u_{12} = \epsilon_w^2 z_1 z_2 f, \tag{3a}$$

where z_i is the distance of the positive charge of dipole i into the oil and

$$f = \frac{2e^2}{4\pi\epsilon_0\epsilon_w\epsilon_h(\epsilon_w + \epsilon_h)r^3} \qquad \text{for } r \gg z_1, z_2,$$

ϵ_0 is the permittivity of vacuum, ϵ_w and ϵ_h are the dielectric constants of water and heptane, respectively. Similarly, if one dipole is in oil and one is in water (Fig. 2 *b*), then

$$u_{12} = \epsilon_w\epsilon_h z_1 z_2 f. \tag{3b}$$

Finally, if both dipoles are in the water phase (Fig. 2 *c*), then,

$$u_{12} = \epsilon_{lr}^2 z_1 z_2 f. \tag{3c}$$

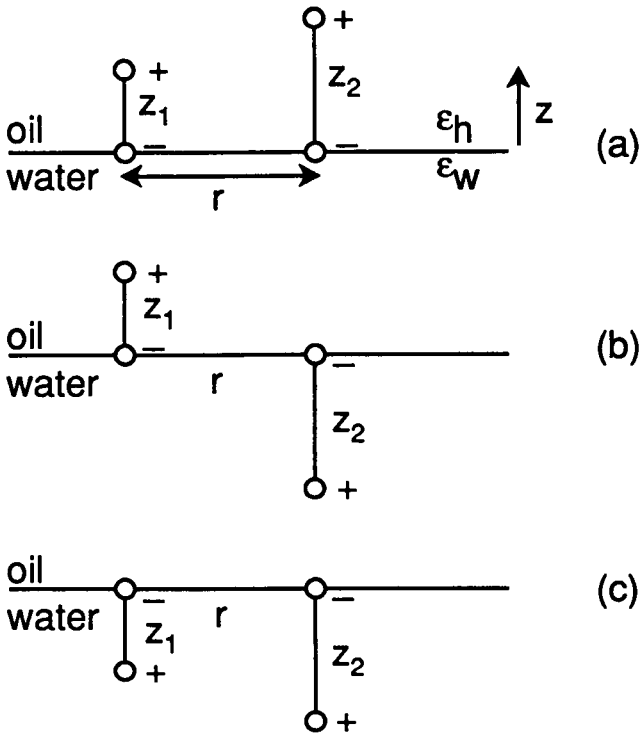

FIGURE 2 Dipole charges at the heptane/water interface with interactions described in Eqs. 3a, b, and c.

Because of the large dielectric ratio $\epsilon_w/\epsilon_h \approx 40$, two dipoles in oil interact with each other far more strongly than two dipoles in water. In the intermediate case, Eq. 3*b*, u_{12} corresponds to an attraction since $z_1 z_2$ is negative. Thus, as shown earlier (2), only the repulsion between dipoles in oil, Eq. 3a, contributes significantly to head group interactions. Furthermore, Eq. 3a shows that this large repulsion in oil is nearly independent of ϵ_w. This is important for the justification of the electrostatic part of our head group model. Because the zwitterionic interactions are very insensitive to the dielectric constant of water and to the location of the negative pole in the water, the only significant features are the dielectric properties of the oil phase and the distance of the positive pole to the interface. In view of the very low solubility of water in heptane it is reasonable to assume that the interface is molecularly sharp and that heptane is dielectrically uniform up to the interface. We are using literature values of the bulk dielectric constants of water (6) and heptane (7) for ϵ_w and ϵ_h and their temperature dependencies.

Thus, the simplest model is to assume two contributions to head group interactions: (*a*) out-of-plane dipoles as described above, in addition to (*b*) the mutual steric exclusions of area of the headgroups of different molecules (2, 3). For the latter, we model PE and PC head groups as circular hard discs of radius $a = 4$ Å with a central dipole *ez* directed into the water or heptane phase. For this simple model, where $u_{ij}^* = u_{ij}$ in Eq. 2 (see defining Eqs. A23 and A24), we have evaluated B_2 and B_3, by setting $z_i = z > 0$ for the three out-of-plane dipoles; thus,

$$u_{12} = \epsilon_w^2 z^2 f \qquad \text{for } R \geq 2a \tag{4a}$$

$$u_{12} = \infty \qquad \text{for } R < 2a, \tag{4b}$$

and similar equations obtain for u_{13} and u_{23}. The predicted second and third virial coefficients are plotted versus z in Fig. 3 (*solid curves*). B_2 does not differ significantly from our earlier results (1). However, improvement in our numerical methods in the present work shows that our previous estimates (1) for B_3 (*triangles* in Fig. 3 *B*), were too low. The earlier results were obtained by means of a numerical integration routine for continuous functions in three dimensions. We previously made an approximation to circumvent the discontinuities inherent in Eq. 4 at $R = 2a = 8$ Å, $s = 8$ Å, and $r = 8$ Å, see Fig. 1. The present results have instead been produced by a better Monte Carlo integration technique (shown by the *solid curve* in Fig. 3 *B*, and described in Appendix *B*). This technique is well suited for integrating discontinuous functions, gives more accu-

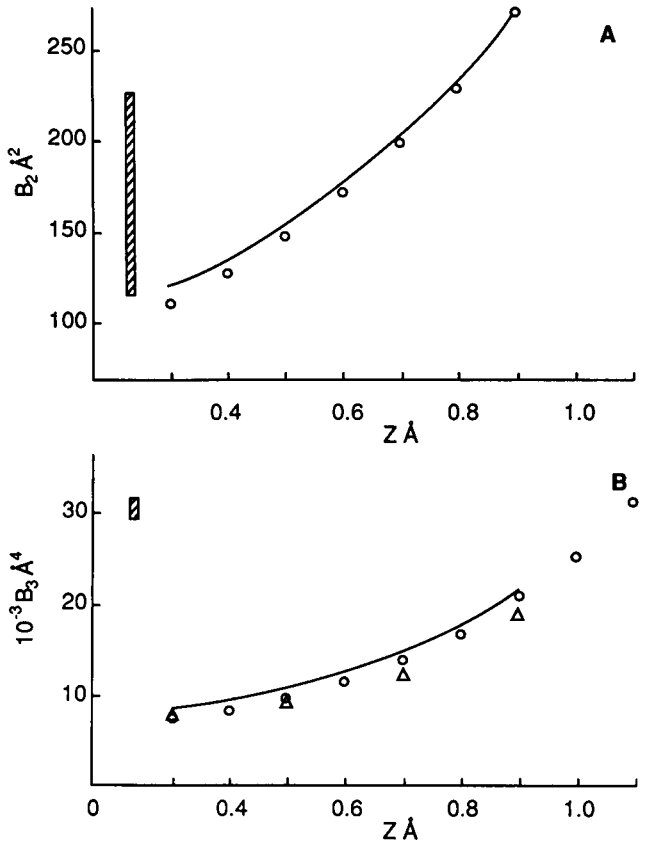

FIGURE 3 Comparison of B_2 and B_3 (*upper and lower panels*, respectively) derived from experiments on $diC_{18}PC$ with results from various models as a function of out-of-plane dipole length z. (*Shaded vertical bars*) experiments, from Table 1. (*Full curves*) present results for simple head group model (hard disc with 4 Å radius and central out-of-plane dipole ez). (*Open circles*) above model with additional in-plane dipole component as shown in Fig. 4.(*Triangles in lower panel*) earlier results (2) for simple model, see text.

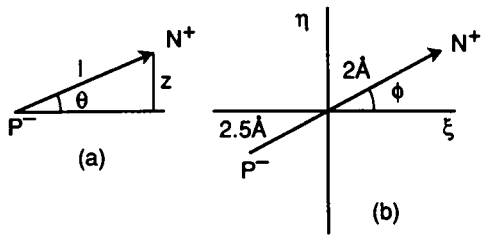

FIGURE 4 Coordinates for model of PC head group with P^- and N^+ charges giving (*a*) out-of-plane dipole moment $ez = el \sin\theta$ with $l = 4.5$ Å and (*b*) in-plane dipole moment $el \cos\theta$. Charges may rotate through angle ϕ in the ξ,η interface.

rate results, and was employed also for the six dimensional integrations reported below.

We now consider a more elaborate head group model in which the P^- and N^+ charges are placed off center on the hard disc with radius 4 Å. This model, thus, includes also in-plane dipolar interactions, as well as steric repulsion and out-of-plane dipolar interactions. In this case the P^-N^+ vector of length $l = 4.5$ Å is defined by a constant tilt angle θ, and a variable rotation angle ϕ in the ξ, η interface (see Fig. 4). The pair potentials u_{ij} in Eqs. 2, A23, and A24 were derived as reported previously (2), using the full set of coordinates given in Table 3 of reference 2. In the evaluation of B_2 and B_3, the normalized angular integrations in Eqs. A23 and A24 were carried out over angles $(\alpha) = \phi/2\pi$ from 0 to 1, for various tilt angles θ, corresponding to $z = 0.3$ to 1.1 Å. The results are shown in Fig. 3 as open circles. For B_2 the present data coincide with those reported earlier for this model (2). Compared with the solid lines for the hard disc and out-of-plane dipole, adding the in-plane dipole component provides a net attraction which decreases both B_2 and B_3. The decrease is small in both cases, consistent with our previous conclusion (2) that the dipole component parallel to the interface may be neglected.

The simple models described above cannot satisfactorily account for both B_2 and B_3. The comparison of experiments with these models is shown in Fig. 3. The experimental range of B_2, shown as a shaded vertical bar on the left side of Fig. 3 *A*, corresponds to the theoretical model (*solid line*) with $z = 0.3$ to 0.9 Å. For these z values the model predicts B_3 values (*solid line* in Fig. 3 *B*) from 9,000 to 18,000 Å^4, much smaller than the experimental results which cluster around $B_3 = 30{,}000$ Å^4 (see the *shaded vertical bar* in Fig. 3 *B*). The comparison with the PE data in Table 2 is equally unsatisfactory. Here the experimental value, $B_2 \sim 120$ Å^2, corresponds to $z \sim 0.3$ Å, which leads to $B_3 \sim 8{,}000$ Å^4, much smaller than the experimental values of $B_3 \sim 20{,}000$ Å^4. In summary, there are two problems with the simple model predictions of B_3. First, the experimental B_3 values for both PE and PC are much larger than predicted by the simple models and, second, for PC the experimental B_3 values are essentially independent of temperature whereas the model that is consistent with B_2 predicts a substantial dependence on temperature. Previous work (3) introduced a molecular model of the PC head group with dipole fluctuations to explain the variation of B_2 with temperature. As shown below, with such fluctuations of the out-of-plane P^-N^+ dipole component the predicted B_3's disagree even more with the experiments.

It is obvious that the theoretical model of a dipole attached to a circular disc is fundamentally insufficient to account for the behavior of the third virial coefficient. An explanation of the failure to fit experimental B_3 data might be the neglect of head group shape in the simple

model. Although this shape effect on B_2 was found to be small (2), the possible shape effect on B_3 might still be considerable. However, as shown below, this is not the case. Instead, it is necessary to introduce an attractive interaction between the head groups. A comparison is made below of the experimental and theoretical ratios of the second and third virial coefficients. This provides evidence that the models considered so far are too simple, and that nondipolar attractions are significant.

ATTRACTIVE INTERACTIONS

It is well known (8) that for noninteracting hard discs $B_3 = 0.782\, B_2^2$. Tables 1 and 2 show that for PC and PE experimental ratios B_3/B_2^2 are much higher than 0.782. To understand these large experimental ratios we have investigated hard discs with radius a, with an in-plane dipole as in Fig. 4 *b*, and with an added short range interaction potential u which depends on the angular orientation of the two discs, as shown in Fig. 5 for three different cases. The discs are free to rotate. Whenever the connecting center line of length r crosses a shaded area of each disc the extra pair potential is

$$u = u_0 e^{-(r-2a)/3} \qquad r \geq 2a, \tag{5}$$

but $u = 0$ if the center line crosses one or two unshaded sections on the discs. For computational reasons we have chosen in Eq. 5, a smoothly varying potential with exponential decay. The decay length is taken equal to the size of a water molecule, 3 Å.

For the models in Fig. 5 we have assumed the discs have radius $a = 5.5$ Å and we have explored a range of u_0 values in Eq. 5. When u_0 increases from very negative (attractive) to very positive (repulsive), B_2 increases from 50 to 300 Å^2. A plot of the results for B_3/B_2^2 versus B_2 in Fig. 6 shows several interesting features. (*a*) A repulsive potential as in Fig. 5 *c* has the same effect as stretching the circular disc into an ellipsoidal shape. According to Fig. 6, such stretching lowers the B_3/B_2^2 ratio. Therefore, the high experimental ratios cannot be due to an asymmetric shape of the head groups or to an extra (nondipolar) short range repulsion between them.

TABLE 1. **Two-dimensional pressure virial coefficients in PC monolayers at 0.01 M NaCl:heptane interfaces**

T°C	B_2,Å^2	$B_3 \times 10^{-3}$, Å^4	B_3/B_2^2
5	115.3	29.3	2.20
10	133.5	31.4	1.76
15	155.0	31.5	1.31
20	177.6	30.2	0.957
25	226.6	31.2	0.608

TABLE 2. **Two-dimensional pressure virial coefficients in PE monolayers at aqueous NaCl: heptane interfaces**

T°C	M_{NaCl}	B_2,Å^2	$B_3 \times 10^{-3}$, Å^4	B_3/B_2^2
5	0.01	127.6	20.0	1.23
20	0.01	111.0	22.2	1.80
20	0.1	123.6	20.0	1.31

(*b*) The results for the various models cluster around the same curve, indicating that B_3/B_2^2 is rather insensitive to angular averaging of the interaction potential. This confirms the previous conclusion (2) that a head-group model with circular symmetry, as in Fig. 5 *a*, is a good approximation for computing virial coefficients. (*c*) In general, repulsion lowers B_3/B_2^2 below 0.782, the ratio for discs with steric hindrance only, and attraction increases the ratio above 0.782. Thus, the high experimental B_3/B_2^2 values in Tables 1 and 2 are compelling

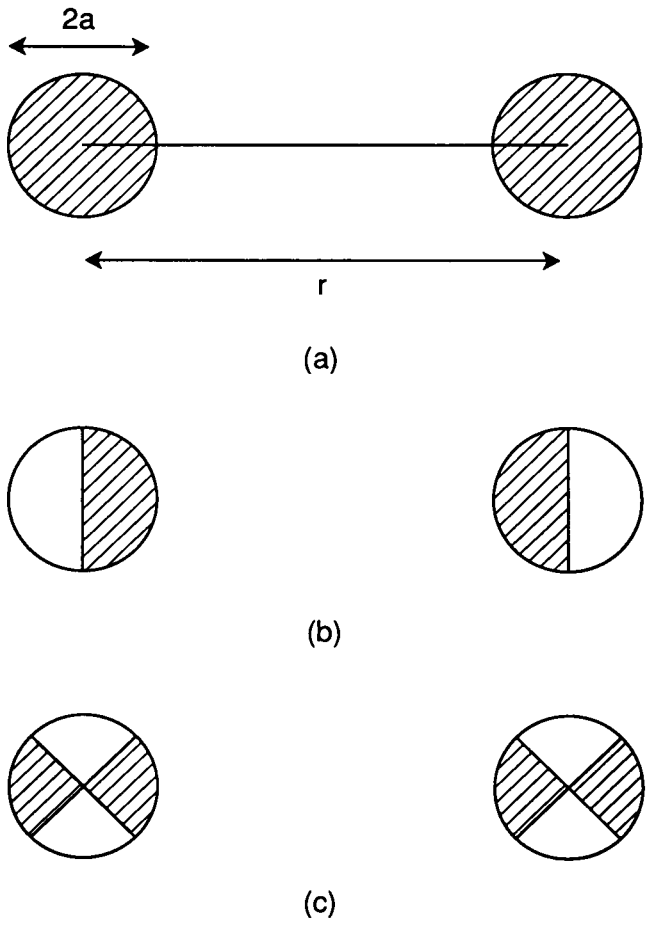

FIGURE 5 Freely rotating discs with pair potential given by Eq. 5 if line connecting centers passes through shaded area of each disc.

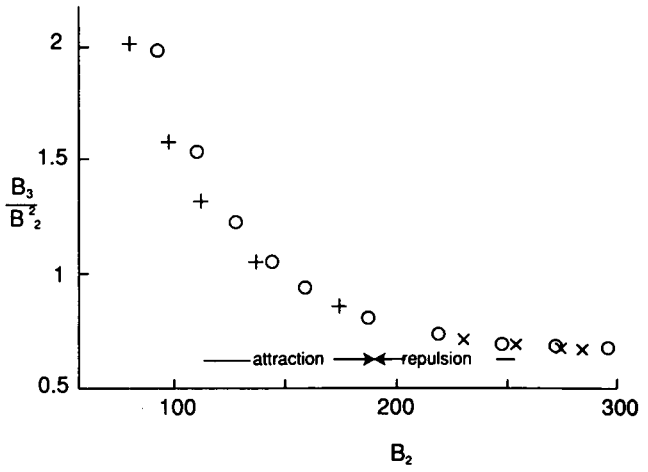

FIGURE 6 Ratio B_3/B_2^2 vs B_2 for head group discs with radius a = 5.5 Å and attractive or repulsive interaction according to Eq. 5. O: model of Fig. 5 *a*; +: model of Fig. 5 *b*; X: model of Fig. 5 *c*.

TABLE 3. **Second and third virial coefficients for disclike head groups with radius a, in-plane dipole as in Fig. 4 with z = 0.2 Å, and attraction as in Fig. 5 a and Eq. 5 with contact potential u_0**

aÅ	u_0/kT	B_2Å^2	B_3Å^4
5.6	−0.50	131.3	20,915
5.6	−0.54	124.6	20,312
5.6	−0.58	118.3	19,955
6.3	−0.93	119.4	29,160
6.3	−0.95	115.2	28,664
6.3	−0.97	111.8	28,600
6.4	−1.03	119.7	30,685
6.4	−1.05	115.7	30,145
6.4	−1.07	112.3	30,183

evidence of attraction between head groups in PC and PE monolayers.

There are several possible origins of head-group attractions that may be important and that are neglected in the simple models above. "Like" species tend to attract in solution due to van der Waals interactions. PE head groups may associate through hydrogen bonding, and PC head groups may associate in water due to hydrophobic interactions among the methylated N^+ ends. Therefore, we describe below the addition of a short-ranged attraction to the simple model. At the same time, we make two small changes to the model parameters for the steric and dipolar interactions to make the model more realistic. First, we also include the small additional repulsion due to the dipoles of the ester linkages in the head groups. For this, we assume an out-of-plane dipole moment of 1 debye per head group, see earlier discussion (2), that we model as an extra contribution of 0.2 Å to the distance z of N^+ into the heptane phase. Second, we assume a slightly larger hard disc radius. The disc radius of 4 Å assumed previously (2) was derived from the molecular area in condensed PC monolayers in crystals at high surface densities. In dilute monolayers, they are not packed so tightly. We now use a slightly larger steric radius as described below.

The simplest case to consider first is PE because it does not have the complex strong dipolar repulsions that PC has. We model the short-ranged pair attraction as a potential u_0 as in Eq. 5. We assume circular symmetry, i.e., no angular dependence; see Fig. 5 *a*. Table 3 shows the predictions for several values of the disc radius a, and contact potential u_0. From Table 3 it is evident that B_2 and B_3 are quite sensitive to changes in a and u_0. The experimental second and third virial coefficients for PE are best accounted for by using the values a = 5.6 Å and $u_0 = -0.54$ kT. This head group radius is reasonable; the contact potential is smaller than expected for a hydrogen bond of several kT because the directionality of hydrogen bonding has been neglected in the present head group model with circular symmetry.

Next we consider the model of the PC head group; this is a modification of the earlier model (3). We represent the PC dipole by the P^- charge and, at 4.5 Å distance, the N^+ charge which is buried at the center of a hydrophobic sphere with radius t = 3.5 Å, the van der Waals radius of the methylated N^+ group. The P^- charge is anchored at the interface and the PN dipole of fixed length may tilt relative to the plane of the interface. The position of the N^+ charge is z Å from the interface into the oil. Fluctuations of z and the average position, z_0, of N^+ are determined by the sum of the hydrophobic free energy, F_h, and the electrostatic free energy, F_e, of the N^+-methylated hydrophobic sphere as a function of z. When the sphere crosses from heptane into water the increase in hydrophobic free energy of the system is

$$F_h = c_1\left(1 - \frac{z}{t}\right) - \frac{c_1}{2}\left(1 - \frac{z^2}{t^2}\right) \qquad t > z > -t. \tag{6}$$

The first term is proportional to the gain in sphere/water contact area which is $2\pi t^2(1 - z/t)$. The second term is proportional to the oil/water interfacial area displaced by the crossing sphere, maximal πt^2 for $z = 0$. The latter contribution to F_h was omitted earlier (3). We are indebted to Prof. George M. Bell of the University of London for calling it to our attention. As before (3), the constant c_1 in Eq. 6 and its temperature dependence are derived from the free energy of transfer of hydrophobic amines from oil into water (9). The (Born) electrostatic free energy of the N^+ charge is approximated as before

(3) by

$$F_e = d_0 + d_1 \frac{z}{t + \Delta z} + d_2 \left(\frac{z}{t + \Delta z}\right)^2 \qquad t > z > -t, \quad (7)$$

where the coefficients d_0, d_1, and d_2 are functions of the bulk dielectric constants of water and heptane, and Δz accounts for how the interfacial "thickness" (i.e., due to fluctuations) modifies the electric field and hence the Born energy as discussed earlier (3). The total free energy of head group orientation, $F_t = F_h + F_e$, is given by

$$F_t = \left(d_0 + \frac{c_1}{2}\right) + \left(\frac{d_1}{t + \Delta z} - \frac{c_1}{t}\right) z + \left(\frac{d_2}{(t + \Delta z)^2} + \frac{c_1}{2t^2}\right) z^2 \qquad t > z > -t. \quad (8)$$

The free energy F_t and its hydrophobic and electrostatic components are plotted versus z in Fig. 7, from Eqs. 6, 7 and 8 with Δz = 3 Å. The component free energies are shown as solid curves for 25°C and the total free energies F_t are shown for 25°C and 5°C. With increasing temperature the minimum of the F_t curve shifts toward higher z. The increasing penetration of the $-N^+(CH_3)_3$ group into the heptane with temperature has two effects on the lateral interaction between the head groups. First, the dipolar repulsion becomes stronger, as is evident from Eq. 3 *a*. Second, the short-ranged head group attraction (see Eq. 5) becomes weaker because the contact area with water of each hydrophobic sphere becomes smaller with increasing temperature. This is indicated in Fig. 8; only the shaded parts of the spheres are exposed to water. We model this variation in attraction with z in a simple way. The contact area with water per sphere changes as $1 - z/t$. This would give a factor $(1 - z/t)^2$ in u_0. However, due to curvature, only a fraction of the surface area of the hydrophobic spheres is effective in short range attraction. Therefore, we assume a quadratic dependence of u_0 on the average position, z_0, of the spheres,

$$u_0 = u_{00}(1 - g|z_0|z_0). \quad (9)$$

We compare the effects on B_2 of the three different functions $u_0(z)$ shown in Fig. 9: (*a*) A constant u_0, (*b*) an approximately linear change of u_0, as $(1 - z_0/t)^2$, and (*c*) a quadratic dependence on z_0 as in Eq. 9. We substitute

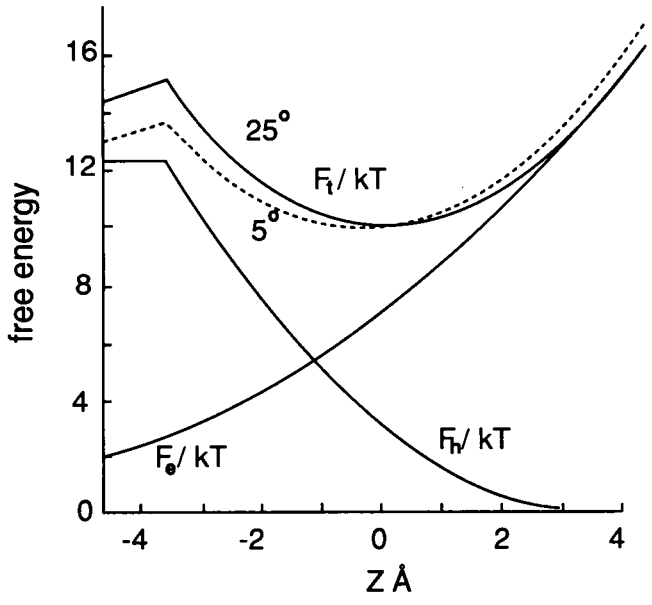

FIGURE 7 Free energy functions of charged hydrophobic sphere with radius t = 3.5 Å and charge e in center at distance z Å from heptane/water interface. Hydrophobic free energy F_h from Eq. 6. Electrostatic free energy F_e from Eq. 7 for average interfacial fluctuations Δz = 3 Å. Total free energy F_t from Eq. 8. (*Solid curves*) 25°C, (*dashed curve*) 5°C.

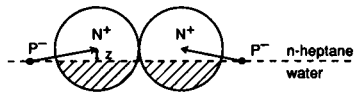

FIGURE 8 Two model head groups in contact at heptane/water interface. Shaded surface in water.

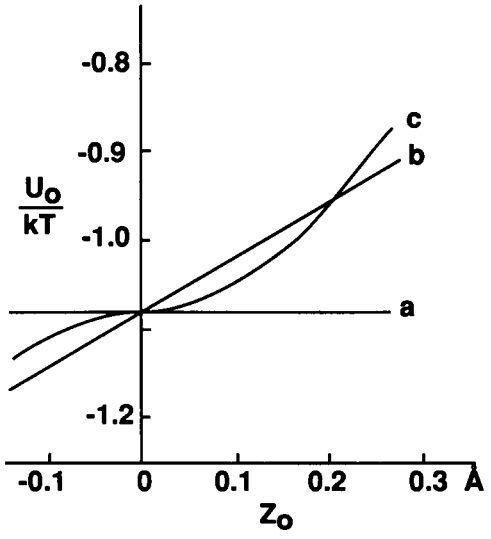

FIGURE 9 Attractive contact potentials u_0 between two head groups at interface as a function of average distance z_0 of N^+ into heptane. (*a*) u_0 = constant; (*b*) $u_0/kT = -1.08(1 - z_0/t)^2$ with t = 3.5 Å; (*c*) $u_0/kT = -1.08(1 - 2.6|z_0|\, z_0)$.

these functions in Eq. 5, add to each short range attraction the same dipole interaction and evaluate B_2 as discussed below. The three resulting curves for B_2 are plotted as a function of temperature and compared with experimental results in Fig. 10. The experimental $B_2(T)$ values suggest a curvature which is reproduced only by the most realistic form of u_0, Eq. 9. It is possible to construct contact potentials $u_0(z_0)$ which give a perfect fit with the experimental data. However, in view of the uncertainty of the experimental B_2 values, and for the sake of simplicity, we have used curve c in the work below. The values we use in Eqs. 5 and 9 are $a = 6.7$ Å, $u_{00} = -1.08$ kT, and $g = 2.6$ Å^{-2}.

FLUCTUATIONS

The interaction between head groups, required to evaluate B_2 and B_3, depends on their mutual distances, average orientation, and is subject to fluctuations of various kinds. In the earlier analysis (3) we introduced the fluctuations of the out-of-plane head group dipole, that is, the N^+ position as given by the free energy $F_t(z)$ of Eq. 8 and illustrated in Fig. 7. The fluctuation energy F_t was identified with the potentials u_i and u_j in Eq. A23, that is, with the variable part of the adsorption potential of the lipid, leading to Eq. A17 in Appendix A. By means of Eq. A23 the dipole interaction $u_{ij}(z_i, z_j)$ from Eq. 3 was properly weighted by the Boltzmann factors of $u_i(z_i) = F_t(z_i)$ and $u_j(z_j) = F_t(z_j)$. We now use the same method for the evaluation of B_3 from Eqs. A21, A23, and A24, using Eqs. 2 and 3 to derive the triplet interaction potential as the sum of the three pair potentials

$$u_{123}(R, s, r, z_1, z_2, z_3) = u_{12}(R, z_1, z_2) + u_{13}(s, z_1, z_3) + u_{23}(r, z_2, z_3). \quad (10)$$

Eq. A21 gives B_3 as a six-dimensional integral which we evaluate numerically with a repeated random choice of the variables R, s, r, z_1, z_2 and z_3 between their integration limits. To improve the convergence of the Monte Carlo integrations we sample integrand space more efficiently by transforming the variables R, s, and r as described in Appendix B. Convergence is enhanced further by approximating the fluctuation potential $F_t(z)$ of Eq. 8 with a square well potential,

$$u_i(z) = F_t = 0 \quad \text{for } z_0 - w < z < z_0 + w$$
$$u_i(z) = F_t = \infty \quad \text{for } z < z_0 - w \text{ and } z > z_0 + w, \quad (11)$$

which is centered on the minimum of F_t at

$$z_0 = \left(\frac{c_1}{t} - \frac{d_1}{t + \Delta z}\right)\left(\frac{c_1}{t^2} + \frac{2d_2}{(t + \Delta z)^2}\right)^{-1}, \quad (12)$$

and with a width $2w$ giving the same mean square fluctuations, μ^2, as the parabolic free energy $F_t(z)$ of Eq. 8. The Eq.,

$$\mu^2 = \frac{\int_{-\infty}^{\infty} (z - z_0)^2 e^{-F_t/kT}\, dz}{\int_{-\infty}^{\infty} e^{-F_t/kT}\, dz}, \quad (13)$$

combined with Eqs. 8 and 11 leads to the relation,

$$w = \left(\frac{c_1}{3t^2} + \frac{2d_2}{3(t + \Delta z)^2}\right)^{-1/2}. \quad (14)$$

To test the quality of the square well approximation we rewrite Eq. 8 in terms of z_0 and w as

$$u_i = F_t(z) = \frac{3}{2w^2}(z - z_0)^2 + \text{constant} \quad (15)$$

We have compared the B_2 values predicted by the square-well and parabolic potentials, Eqs. 11 and 15, for a range of z_0 values, for $w = 2$ Å as corresponds to realistic values from Eq. 14, for head group radius $a = 6.7$ Å, and for pair interactions as discussed above. It was found that the B_2 computed using Eq. 11 is higher than with Eq. 15. This is because the square well potential is more efficient in permitting fluctuations of the head groups to larger z, where there is stronger repulsion and weaker attraction between head groups, than the parabolic potential. The differences are small however, only

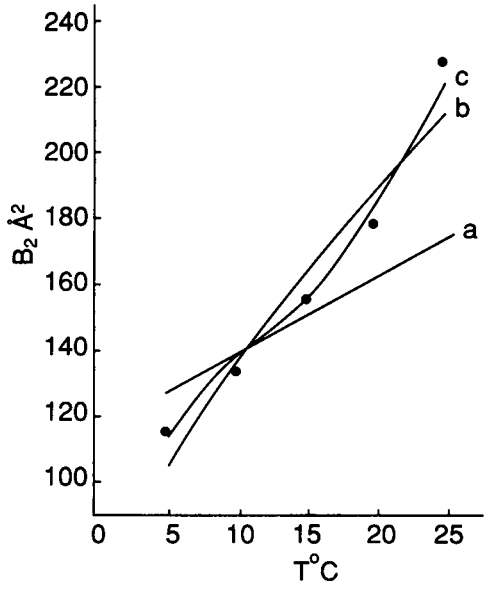

FIGURE 10 B_2 as a function of temperature for attractive contact potentials in Fig. 9 and remaining interactions as described in text. Experimental values as filled circles.

~ 10 Å^2 in B_2 in the range $B_2 = 100$–250 Å^2. This is of the same order as the experimental uncertainty in B_2.

Thus, the model for PC interactions is as follows. The PC head group is represented by a circular disc with radius 6.7 Å, with a central dipole ez, where z is the distance into the heptane which fluctuates in the square well potential of Eq. 11, with z_0 given by Eq. 12, and an additional contribution to z_0 of 0.2 Å to account for the ester dipoles of the head group. The pair interaction between head groups is the sum of excluded area effects, dipole interactions following Eq. 3, and an attractive potential,

$$\frac{u_0(r)}{kT} = -1.08(1 - 2.6z_0^2)e^{-(r-2a)/3}, \qquad (16)$$

due to hydrophobic effects. The results of the computations, plotted versus temperature as triangles in Fig. 11, show that for the above model both B_2 and B_3 are smaller than the experimental values (*filled circles*). This discrepancy is not due to the magnitude of the orientational fluctuations of the head groups; increasing w in Eq. 14 to $w + 0.45$ Å (*crosses* in Fig. 11) leads to higher values of B_2 but lower values of B_3. This discrepancy also remains in the absence of attractions; i.e., when $u_0 = 0$ in Eq. 16. We consider below correlations in fluctuations and show that this leads to predictions consistent with the experiments.

How do the fluctuations affect the virial coefficients? As the N^+ moves more deeply into the oil (i.e., large positive z), it causes large lateral repulsions and diminished attractions, whereas fluctuations of the N^+ into the water phase contribute little to the interactions. Hence, for a given average position z_0 larger dipole fluctuations increase B_2 (Fig. 11, *curves a* and *b*). B_3 depends on triplet interactions, as the sum of three pair potentials (see Eqs. 10, A21 and A24). Here, the correlation between fluctuations is important. For three head groups with independently fluctuating values z_1, z_2 and z_3, the three pair dipole potentials, proportional to the pair products z_1z_2, z_1z_3 and z_2z_3, are not independent of each other. For example, given two large pair interactions, the third pair tends to also be large. We have found, surprisingly, that such correlated dipole interactions are not pairwise additive after averaging with respect to fluctuations. That is, assuming additivity of the instantaneous pair potentials, Eq. 10, we have evaluated the average interactions with Eqs. A23 and A24 for a number of spatial configurations (R, s, r). For the case under discussion of positively correlated pair potentials the result for all configurations was

$$u^*_{123}(R, s, r) < u^*_{12}(R) + u^*_{13}(s) + u^*_{23}(r). \qquad (17)$$

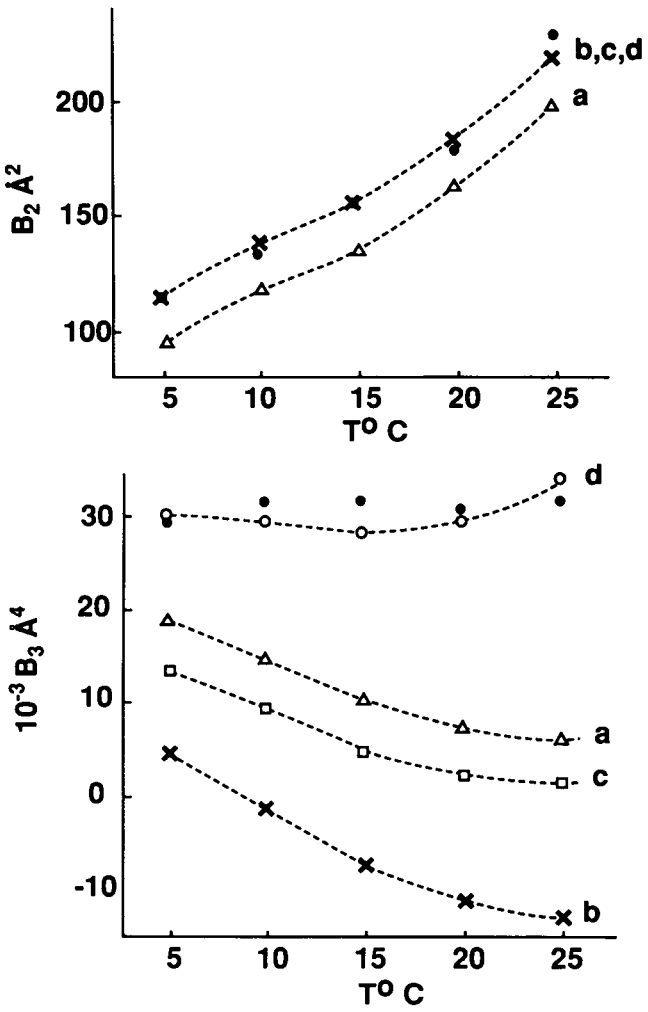

FIGURE 11 B_2 and B_3 as a function of temperature for disc radius a = 6.7 Å, attractive pair potential of Eq. 16, dipole fluctuations as in Eqs. 11, 12, and 14 with extra contribution to z_0 of 0.2 Å for ester dipoles. Curves for variations of fluctuations. (*a*) above model. (*b*) additional contribution of 0.45 Å to w, Eq. 14, for dipole fluctuations. (*c*) with additional independent interfacial fluctuations of Eq. 18 with $w_s = 0.95$ Å. (*d*) with negatively correlated interfacial fluctuations of Eq. 19 with $w_s = 0.95$ Å. (*Filled circles*) experiments.

This inequality leads to a relatively larger term $\exp(-u^*_{123}/kT)$ in Eq. A21 and, hence, decreases B_3, consistent with curves *a* and *b* in the lower part of Fig. 11. The results of the positive correlation among the three pair potentials between three independently fluctuating dipoles is that, relative to pair repulsions, the triplet interaction becomes less repulsive for increasing fluctuations.

We now consider interfacial fluctuations, where we distinguish two separate effects. The first effect, as argued earlier (3), is on the change of the self-energy of the N^+ charge as it passes from water into the heptane

phase. The average widening of the interfacial region, due to fluctuations, has been simulated as before (3) by "stretching" the middle part of the $F_t - z$ curve with the introduction of the thickness parameter $\Delta z = 3$ Å in Eq. 8. We now consider also the extra fluctuation of the dipole component of each pair potential u_{ij}, arising from the influence of the fluctuating shape of the interface between the two head groups on their dipole interaction. Eq. 3 holds for a planar interface. If, however, the interface between two head groups bulges toward oil or toward water, the dipole interaction will be changed in a way which is difficult to evaluate but, considering Eqs. 3a and c, for positive and negative interfacial deformations the interaction will change in an asymmetrical way. Such an asymmetry may be introduced with three independent random fluctuations Δ_{12}, Δ_{13}, and Δ_{23} of the z values which enter the pair potentials in Eq. 3 as follows: $(z_1 + \Delta_{12})(z_2 + \Delta_{12})$ in u_{12}, $(z_1 + \Delta_{13})(z_3 + \Delta_{13})$ in u_{13}, $(z_2 + \Delta_{23})(z_3 + \Delta_{23})$ in u_{23}.

We have generated the three fluctuations Δ_{ij} between $-w_s$ and $+w_s$, for a square well potential as in Eq. 11, and using three random numbers R_n from a random number generator which is uniform between 0 and 1

$$\Delta_{ij} = -w_s + 2w_s R_n. \tag{18}$$

The effects of such independent potential fluctuations are shown for $w_s = 0.95$ Å by the difference between curves *a* and *c* in Fig. 11. The increase of B_2 from curve *a* to *c* is essentially the same as that of enhancing w by 0.45 Å, curve *a* to *b*. The change of B_3, however, is quite different. Whereas the additional, positively correlated fluctuations of the dipole potentials decreased B_3 from curve *a* to *b*, adding the uncorrelated fluctuations of Eq. 18 decreases B_3 much less, only from curve *a* to *c*.

Finally, instead of uncorrelated fluctuations, we consider negative correlation between the three pair potentials in B_3 subject to interfacial fluctuations. In the computations we first generate three independent fluctuations $\Delta_i = -w_s + 2w_s R_n$ as in Eq. 18. We then take three linear combinations in whose sum each Δ_i vanishes to produce three negatively correlated fluctuations Δ_{ij}

$$\begin{aligned}\Delta_{12} &= \Delta_1/4 + \Delta_2/4 - \Delta_3/2\\ \Delta_{13} &= -\Delta_1/2 + \Delta_2/4 + \Delta_3/4\\ \Delta_{23} &= \Delta_1/4 - \Delta_2/2 + \Delta_3/4.\end{aligned} \tag{19}$$

We now proceed as before, calculating the pair potentials with $(z_1 + \Delta_{12})(z_2 + \Delta_{12})$ in u_{12} et cetera. Results are shown in Fig. 11 for $w_s = 0.95$ Å as curves *d*. For the present model, we find large positive values of B_3, obviously the result of the negative correlations among the pair potentials. For B_2 the curves *c* and *d* coincide because for the single pair interaction of B_2 the fluctuations Δ_{12} of Eq. 19 remain random. Some negative correlation between the triplet pair potentials is not unreasonable. Because the three dipole pairs are contiguous, the instantaneous fluctuations of the intervening interface are unlikely to be always in the same direction but, rather, in opposite direction between different pairs at least part of the time. In a more formal argument, the interfacial area relevant to triplet interaction is larger than that relevant to pair interaction and, hence, the average fluctuations are smaller for the triplet than for the pair interaction.

We have demonstrated in Fig. 11 that, while head group and interfacial fluctuations both increase B_2, their influence on B_3 is opposite. Therefore, a combination of the two types of fluctuations can explain the experimental B_2 and B_3 data. The parameters for curve *d* in Fig. 11 fit the experimental data for B_2 and B_3 probably within the experimental errors. This set of parameters is not unique however, and the agreement with experimental values can possibly be improved. Besides, accounting for fluctuations in the hydrophobic attractions might shift the parameter values somewhat. However, in view of the approximate nature of our (circularly averaged) hydrophobic potential function of Eq. 16, such a refinement is probably not justified.

DISCUSSION

The present head group model of PC has been derived to explain the lateral pressure of monolayers at the *n*-heptane/water interface. We have tested this model also against the change of the interfacial potential, ΔV, with coverage. The initial slope of the $\Delta V - \Gamma$ curve yields the average ratio of the total dipole length per head group and dielectric constant, $\langle d/\epsilon \rangle$, which increases for PC by 0.025 Å between 10° and 20° C (1). For three similar dipole fluctuation potentials we have compared this result with the temperature dependent contribution of the P^-N^+ dipole by computing the average value $\langle z/\epsilon \rangle$ as a function of temperature. For the square well potential of eq. 11 the increase of $\langle z/\epsilon \rangle$ between 10° and 20°C is 0.053 Å, for the parabolic well potential of Eq. 15 we find 0.054 Å, and the asymmetric fluctuation potential of Fig. 7 yields 0.115 Å. The differences between these results show how sensitive the computation of $\langle z/\epsilon \rangle$ is to the model. It is encouraging that the theoretical and experimental results are of the same order of magnitude.

We have shown that, to explain the observed lateral head-group interactions, one needs to consider between PE head groups: (*a*) steric repulsion and (*b*) attraction due to hydrogen bonding. Between PC head groups we have: (*a*) steric repulsion, (*b*) attraction decreasing with temperature caused by hydrophobic effects, (*c*) dipolar

repulsion increasing with temperature and (d) out-of-plane fluctuations of head groups and of interface leading to positive and negative correlations between dipole interactions in triplet clusters. In the overall lateral head-group interactions the above contributions are all of the same magnitude, although in the case of PC the dipole fields dominate long-range interactions.

In the earlier work (2, 3) we developed a head-group model for dilute PC and PE monolayers at the oil/water interface. The present extended analysis of the lateral pressure and the near-linearity of the surface potential with lipid concentration (1) are good evidence of the essential invariance of the head-group orientation up to the gas/liquid phase transition in the monolayers. We believe that the main features of our head group model carry over to the higher packing densities in phospholipid bilayers and membranes. This is consistent with results on head group orientation in PC membranes obtained by Seelig and coworkers (10–12) using NMR to measure quadrupole splitting in selectively deuterated samples. They conclude that the incorporation of phloretin into PC membranes changes the choline orientation such that the N^+ end of the P^-N^+ dipoles moves toward the hydrocarbon layer, partly compensating the electrostatic field of the phloretin dipole (10). Parallel changes have been measured upon the adsorption of negative ions to PC membranes (11). It is interesting that these NMR spectral changes are in the same direction as observed earlier with increasing temperature (12). Therefore, in a qualitative sense these NMR studies are consistent with our model of the PC head group from monolayer pressures.

The NMR data above are interpreted in terms of order parameters which, unfortunately, are difficult to relate to an overall tilt of the choline moiety with respect to the bilayer plane. There is, of course, a difference in molecular packing between monolayers and bilayers. The bilayer/water interface is rougher than the oil/water interface. Therefore, the average tilt of the head group dipoles may well differ in the two cases, the common feature being the propensity of the methylated N^+ end of the PC head group to move into the hydrocarbon phase, increasingly so at increasing temperatures. Actually, the recent x-ray and neutron scattering analysis of PC bilayers by Wiener and White (13) places the choline group on average slightly further away from the bilayer center than the phosphate group. The positions are subject to large fluctuations. The analysis does not differentiate between random and concerted fluctuations and no temperature effects were included in this study done at 23°C on partially hydrated bilayers.

The temperature dependence of the dipolar head group repulsion is consistent with the repulsion between PC bilayers which reportedly is greater at 50°C than at 25°C (14). Thus, it is likely that the perpendicular repulsion between lipids in adjacent bilayers has the same molecular origin as the lateral repulsions among phospholipids. There are several theories and simulations of the interaction between bilayers, as reviewed e.g. by Granfeldt and Miklavic (15), but these studies fail to address the large difference in behavior between PE and PC and the large temperature dependence of PC bilayers (14). Because these important features are well explained by our molecular head group models in the case of lateral head group interaction, it is of interest to study the interaction between phospholipid bilayers with the same or similar head group models.

APPENDIX A

Derivation of the interfacial virial expansion

Hill (4) has developed the formally exact "two-dimensional" virial expansion of the lateral pressure (or surface pressure), Π, of a monatomic gas adsorbed to a solid surface. We extend his work in two ways. First, instead of a monatomic gas, we consider the adsorption of diatomic (dipolar) molecules. Second, we carry the virial expansion beyond B_2 to include B_3.

The interaction potential between diatomic molecules depends not only on their relative position, but also on one or more internal coordinates. It is convenient to normalize the set of internal coordinates, $(\alpha)_i$ of molecule i. For example, in the case of the rigid rotator of length l in Fig. A1, representing a dipolar molecule, we have,

$$\int d(\alpha) = \int_0^{2\pi} \int_0^{\pi} \frac{1}{4\pi} \sin\theta \, d\theta d\phi = 1. \qquad \text{(A1)}$$

The set of position coordinates (x) refers to one end, P, of the molecule

$$d(x) = d\xi_P d\eta_P d\zeta_P. \qquad \text{(A2)}$$

When the ξ,η plane in Fig. A1 indicates the adsorbing solid surface, the adsorption potential u_i of a gas molecule i depends on $(\alpha)_i$ and on its distance ζ_i from the solid. The pair potential, u_{12} between two molecules depends on $(x, \alpha)_1$ and $(x, \alpha)_2$, the interaction potential between three molecules, u_{123}, depends in addition on $(x, \alpha)_3$.

Let the adsorbing ξ,η plane, with area $\int d\xi d_\eta = A$, be in contact with the diatomic gas with volume $\int d\xi d\eta d\zeta = V$, temperature T,

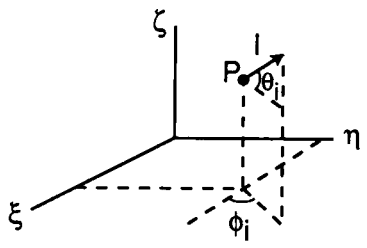

FIGURE A1 Coordinates for diatomic molecule near ξ,η interface.

chemical potential μ. We use expansions in powers of the activity z of the gas,

$$z = \text{constant}\, e^{\mu/kT}, \tag{A3}$$

where the constant is chosen such that z equals the concentration (number density) ρ of the gas without interactions, that is, $z \to \rho$ when $\rho \to 0$.

We start with Hill's formal results (4) for the lateral pressure Π and for the total amount adsorbed ΓA (Gibbs definition of surface excess),

$$\frac{\Pi A}{kT} = \sum_{j\geq 1} V(b_j - b_j^0)z^j \tag{A4}$$

$$\Gamma A = \sum_{j\geq 1} Vj(b_j - b_j^0)z^j, \tag{A5}$$

where superscript 0 indicates absence of the adsorbing surface. The b_j's are related to the configuration integrals, Z_N for N molecules in V,

$$b_1 = \frac{Z_1}{V} \tag{A6}$$

$$b_2 = \frac{Z_2 - Z_1^2}{2V} \tag{A7}$$

$$b_3 = \frac{Z_3 - 3Z_1Z_2 + 2Z_1^3}{6V} \tag{A8}$$

with the same expressions for the b_j^0's in terms of the Z_N^0's for the system without adsorption.

The specifics of the system enter into the configuration integrals with the interaction potentials u, introduced above, between molecules and with the adsorbing surface. We allow for an influence of the adsorbing solid on the intermolecular potentials, that is, $u_{12} \neq u_{12}^0$ and $u_{123} \neq u_{123}^0$.

$$Z_1^0 = V \tag{A9}$$

$$Z_2^0 = \int e^{-u_{12}^0/kT}\, d(x)_1 d(x)_2 d(\alpha)_1 d(\alpha)_2 \tag{A10}$$

$$Z_3^0 = \int e^{-u_{123}^0/kT}\, d(x)_1 d(x)_2 d(x)_3 d(\alpha)_1 d(\alpha)_2 d(\alpha)_3 \tag{A11}$$

$$Z_1 = \int e^{-u_1/kT}\, d(x)_1 d(\alpha)_1 \tag{A12}$$

$$Z_2 = \int e^{-(u_1+u_2+u_{12})/kT}\, d(x)_1 d(x)_2 d(\alpha)_1 d(\alpha)_2 \tag{A13}$$

$$Z_3 = \int e^{-(u_1+u_2+u_3+u_{123})/kT} \times d(x)_1 d(x)_2 d(x)_3 d(\alpha)_1 d(\alpha)_2 d(\alpha)_3. \tag{A14}$$

Reversion of the series in Eq. A5, substitution for z in Eq. A4, and using Eqs. A6 to A14 yields the two dimensional virial expansion, Eq. 1, with three-dimensional expressions for the virial coefficients,

$$B_2 = -\frac{A}{2}\int [e^{-(u_1+u_2)/kT}(e^{-u_{12}/kT} - 1) - e^{-u_{12}^0/kT} + 1] \times d(x)_1 d(x)_2 d(\alpha)_1 d(\alpha)_2 \times [\int (e^{-u_1/kT} - 1)\, d(x)_1 d(\alpha)_1]^{-2} \tag{A15}$$

$$B_3 = 4B_2^2 - \frac{A^2}{3} \times \int [e^{-(u_1+u_2+u_3)/kT}(e^{-u_{123}/kT} - 3e^{-u_{12}/kT} + 2) - e^{-u_{123}^0/kT} + 3e^{-u_{12}^0/kT} - 2] \times d(x)_1 d(x)_2 d(x)_3 d(\alpha)_1 d(\alpha)_2 d(\alpha)_3 \times [\int (e^{-u_1/kT} - 1) d(x)_1 d(\alpha)_1]^{-3} \tag{A16}$$

The above results are applied to an aqueous solution bounded by an adsorbing oil/water interface. The only change is that the interaction potentials refer to solute molecules in the presence of the water as solvent, the formal derivation remaining the same.

We specialize to the case of strong adsorption by phospholipids, the rotator in Fig. A1 representing the dipolar head group. Let the adsorption potential u_1 of a lipid molecule i consist of two terms. A large negative term $u_i(\zeta)$ is a delta function at $\zeta = 0$ which keeps the phosphate charge (P in Fig. A1) of an adsorbed lipid molecule at the interface. A small second contribution $u_i(\theta, \phi)$ depends on the orientation of the P^-N^+ head group vector. We assume that for lipid molecules outside the adsorption plane, where $u_i = 0$, the mutual interactions attain the bulk values, $u_{12} = u_{12}^0$ and $u_{123} = u_{123}^0$. In that case contributions to B_2 and B_3 in Eqs. A15 and A16 vanish for $\zeta \neq 0$. At the interface the terms with the large absorption factor(s) $e^{-u_i/kT}$ dominate the integrands in Eqs. A15 and A16 and, hence the other terms, referring to bulk properties, may be omitted. In this case the Eqs. for B_2 and B_3 become

$$B_2 = -\frac{1}{2A} \times \frac{\int e^{-(u_1+u_2)/kT}(e^{-u_{12}/kT} - 1)\, d\xi_1 d\eta_1 d\xi_2 d\eta_2 d(\alpha)_1 d(\alpha)_2}{[\int e^{-u_1/kT} d(\alpha)_1]^2} \tag{A17}$$

$$B_3 = 4B_2^2 - \frac{1}{3A}\int e^{-(u_1+u_2+u_3)/kT}(e^{-u_{123}/kT} - 3e^{-u_{12}/kT} + 2) \times d\xi_1 d\eta_1 d\xi_2 d\eta_2 d\xi_3 d\eta_3 d(\alpha)_1 d(\alpha)_2 d(\alpha)_3 \times [\int e^{-u_1/kT} d(\alpha)_1]^{-3} \tag{A18}$$

The above equations are similar to the expressions for B_2 and B_3 in the three dimensional virial expansion. The difference is that now the integrands are weighted by the Boltzmann factor of the adsorption potentials of the participating molecules, 1 and 2 for B_2, and 1, 2, and 3 for B_3. The normalized Boltzmann factor of molecule i is

$$\frac{e^{-u_i/kT}}{\int e^{-u_i/kT} d(\alpha)_i} \tag{A19}$$

The large negative contribution to u_i, the delta function at the interface, is constant and, hence, cancels in Eq. A19. Only the variable part of u_i, deriving from head-group orientation, enters into the evaluation of B_2 and B_3 to the extent that the potentials u_{12} and u_{123} depend on head group orientation.

It is useful to separate the integrations over distance and angular coordinates. Then Eqs. A17 and A18 become

$$B_2 = -\frac{1}{2}\int_0^\infty (e^{-u_{12}^*/kT} - 1) 2\pi R\, dR \tag{A20}$$

$$B_3 = 4B_2^2 - \tfrac{1}{3}\int (e^{-u_{123}^*/kT} - e^{-u_{12}^*/kT} - e^{-u_{13}^*/kT} - e^{-u_{23}^*/kT} + 2)\, d\tau, \tag{A21}$$

where the integrations with respect to the distances R, s, and r between the head groups, compare Fig. 1, in the volume element $d\tau$ are (1),

$$\int d\tau = \int_0^\infty dR \int_0^\infty ds \int_{|R-s|}^{R+s} \cdot \frac{8\pi Rsr\, dr}{[(R+s+r)(R+s-r)(R-s+r)(-R+s+r)]^{1/2}}. \tag{A22}$$

The integrands in Eqs. A20 and A21 are averages with respect to the angular coordinates $(\alpha)_i$ which determine the potential u_i for orientation of head group dipole i

$$e^{-u_{ij}^*/kT} = \frac{\int e^{-(u_i+u_j+u_{ij})/kT} d(\alpha)_i d(\alpha)_j}{[\int e^{-u_1/kT} d(\alpha)_1]^2} \quad \text{(A23)}$$

$$e^{-u_{123}^*/kT} = \frac{\int e^{-(u_1+u_2+u_3+u_{123})/kT} d(\alpha)_1 d(\alpha)_2 d(\alpha)_3}{[\int e^{-u_1/kT} d(\alpha)_1]^3}. \quad \text{(A24)}$$

APPENDIX B

Monte Carlo integrations

The random number generator (rng) employed a combination of two traditional congruent rng's, as outlined by Knuth (17). This "shuffled linear congruential method" provides a potentially much longer run length than each of the rng's separately before repetition occurs in the pseudo-random sequence of numbers which is generated. Each separate rng had a cyclic run length of order 10^5, with deviations from uniformity up to 6% in the 0 to 1 interval. In the combination rng no significant deviations from uniformity were detected in runs generating up to 10^7 random numbers. As a further test of the rng, Monte Carlo integrations (18) of B_2 were compared with numerical integrations using a three dimensional integration routine based on Simpson's rule (18) in which convergence was tested by doubling the number of equally spaced sampling points in each test cycle. The two methods showed no significant differences for errors as small as 0.1 percent, using sequences of 3×10^6 random numbers.

The numerical integration of B_3 may be made more accurate in several ways. Recognizing the equivalence of R and s in Eq. A22 we modify

$$\int_0^\infty dR \int_0^\infty ds \int_{|R-s|}^{R+s} dr = 2 \int_0^\infty dR \int_0^R ds \int_{R-s}^{R+s} dr, \quad \text{(B1)}$$

Because R and s may be mapped onto cartesian coordinates, we may also use cylindrical coordinates ρ and ω, see Fig. B1, such that $R = \rho \cos \omega$ and $s = \rho \sin \omega$, with the change

$$\int_0^\infty dR \int_0^R ds = \int_0^\infty \rho d\rho \int_0^{\pi/4} d\omega. \quad \text{(B2)}$$

Overlap of the three hard discs with radius a may occur for $\rho < 4a$,

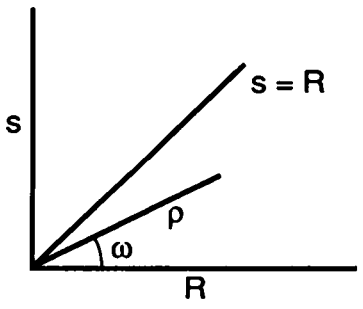

FIGURE B1 Coordinates used in Eqs. B1 and B2.

giving rise to discontinuities in the integrand which are absent for $\rho > 4a$. Therefore, it is convenient to split the integral for B_3 in two parts,

$$\int_0^\infty \rho d\rho = \int_0^{4a} \rho d\rho + \int_{4a}^\infty \rho d\rho. \quad \text{(B3)}$$

The first integral is straightforward, the integrand of the second part is found to decay very slowly, as $1/\rho^2$. For this reason we convert

$$\int_{4a}^\infty \rho d\rho = \int_{1/\rho=0}^{1/4a} \rho^3 d(1/\rho) \quad \text{(B4)}$$

With Eq. B4 the numerically awkward integration limit ∞ is replaced by 0, and the integrand is nearly constant over the entire range of $1/\rho$. For this reason we also change in the third integration in Eq. B1

$$dr = r^2 d(1/r). \quad \text{(B5)}$$

Each term of B_3 was evaluated separately with an appropriate number of integrand values. In all integrations the random number sequence used was divided into ten equal parts and the standard deviation determined by comparing the integral values from each part of the sequence. In the six dimensional integrations for B_3 computer time was the limiting factor in accuracy, which, in Fig. 11 is $\sim 1\%$ in B_3.

We thank Dr. Terrel L. Hill for his help with the material in Appendix A, Dr. Richard P. C. Rogers for providing the random number program, Prof. George M. Bell for his contribution to Eq. 6, and Prof. Stephen White for preprints of his recent work.

We thank North Atlantic Treaty Organization (NATO) and the National Institutes of Health for financial support.

Received for publication 15 April 1991 and in final form 7 January 1992.

REFERENCES

1. Mingins, J., D. Stigter, and K. A. Dill. 1992. Phospholipid interactions in model membrane systems. I. Experiments on monolayers. *Biophys. J.* 61:1603–1615.
2. Stigter, D., and K. A. Dill. 1988. Lateral interactions among phospholipid head groups at the heptane/water interface. *Langmuir.* 4:200–209.
3. Dill, K. A., and D. Stigter. 1988. Lateral interactions among phosphatidylcholine and phosphatidylethanolamine head groups in phospholipid monolayers and bilayers. *Biochemistry.* 27:3446–3453.
4. Hill, T. L. 1959. Relations between different definitions of physical adsorption. *J. Phys. Chem.* 63:456–460.
5. Joslin, C. G. 1982. The second and third virial coefficients of a surface film of hard disc dipoles. *Mol. Phys.* 45:87–96.
6. Harned, H. S., and B. B. Owen. 1958. Physical chemistry of electrolytic solutions. Reinhold, New York. p 160.
7. Smyth, C. P., and W. N. Stoops. 1928. *J. Am. Chem. Soc.* 50:1883.
8. Ree, F. H., and W. G. Hoover. 1967. Seventh virial coefficients for hard spheres and hard disks. *J. Chem. Phys.* 46:4181–4197.
9. Bergstrom, S., and G. Olofsson. 1975. Thermodynamic quantitites for the solution and protonation of four C_6-amines in water over a wide temperature range. *J. Solution Chem.* 4:535–555.

10. Bechinger, B., and J. Seelig. 1991. Interaction of electric dipoles with phospholipid head groups. A ^{2}H and ^{31}P NMR study of phloretin and phloretin analogues in phosphatidylcholine membranes. *Biochemistry.* 30:3923–3929.

11. Scherer, P. G., and J. Seelig. 1989. Electric charge effects on phospholipid head groups. Phosphatidylcholine in mixtures with cationic and anionic amphiphiles. *Biochemistry.* 28:7720–7728.

12. Gally, H.-U., W. Niederberger, and J. Seelig. 1975. Conformation and motion of the choline head group in bilayers of dipalmitoyl-3-sn-phosphatidylcholine. *Biochemistry.* 14:3647–3652.

13. Wiener, M. C., and S. H. White. 1992. Structure of a fluid dioleoylphosphatidylcholine bilayer determined by joint refinement of x-ray and neutron diffraction data. III. Complete structure. *Biophys. J.* 61:434–447.

14. Rand, R. P. 1981. Interacting phospholipid bilayers: measured forces and structural changes. *Annu. Rev. Biophys. Bioeng.* 10:277–314.

15. Granfeldt, M. K., and S. J. Miklavic. 1991. A simulation study of flexible zwitterionic monolayers. Interlayer interaction and head group conformation. *J. Phys. Chem.* 95:6351–6360.